Available online at www.sciencedirect.com
SCIENCE DIRECT
Catalysis Today 107–108 (2005) 663–670
CATALYSIS TODAY
www.elsevier.com/locate/cattod

Influence of rare earth elements La, Nd and Yb on the acidity of H-MCM-22 and H-Beta zeolites

Angela Martins [a], João M. Silva [a], Carlos Henriques [b], Fernando Ramôa Ribeiro [b], M. Filipa Ribeiro [b,*]

[a] *Departamento de Engenharia Química, Instituto Superior de Engenharia de Lisboa, R. Conselheiro Emídio Navarro, 1950-062 Lisboa, Portugal*
[b] *Departamento de Engenharia Química, Instituto Superior Técnico, Av. Rovisco Pais, 1049-001 Lisboa, Portugal*

Available online 25 August 2005

Abstract

The influence of rare earth (RE) elements on the acidic properties of H-MCM-22 and H-Beta was studied by pyridine adsorption followed by infrared spectroscopy (FTIR) and *n*-heptane cracking, as a model reaction.

The zeolites were submitted to ion exchange with rare earth nitrate solutions of La, Nd and Yb. The FTIR spectra of REH-MCM-22 indicate the presence of RE elements inside supercages and in the sinusoidal channels of the zeolite. After pyridine adsorption two additional bands are detected in REH-MCM-22 and REH-Beta, related to pyridine bonded to RE^{3+} cations.

The *n*-heptane cracking reaction shows that the effect of rare earth elements is related not only to the acidity but also with the porous structure of both zeolites. In H-Beta zeolite, the presence of RE elements enhances the acidity of the catalysts. In H-MCM-22 zeolite, the most relevant effect of rare earth elements is on the shape selectivity that becomes more pronounced with the ionic radius of the RE elements. The nature of the coke deposited on the two materials shows distinct profiles that are also related to its porous structure.

Keywords: H-Beta; H-MCM-22; Rare earth elements; Acidity; Pyridine; *n*-Heptane cracking; Coke deposition

1. Introduction

Rare earth (RE) elements play an important role in the modification of some catalysts, namely faujasites, raising its stability and activity in cracking reactions [1]. The presence of rare earth cations enhances the catalyst activity as a consequence of a higher concentration in Brönsted acid sites because of the hydrolysis of water of solvation of RE^{3+} cations that takes place in the zeolitic cavities [2]. The introduction of rare earth elements also prevents aluminum loss from the zeolite structure, thus resulting in enhanced structural resistance to the severe hydrothermal conditions found in the regeneration step of the FCC [3]. Furthermore, the presence of highly charged cationic species can also modify the acid strength distribution in the zeolite due to the polarization of OH groups or to an inductive effect on these groups [1].

The influence of rare earth elements on faujasites is well studied, mainly on cracking reactions [3–5], but also in other reactions like hydrogen transfer [6] and isomerization reactions [7,8]. The increase of faujasite catalysts performances led us to study the effect of the introduction of RE elements on other zeolite structures. Nevertheless, there are only a few studies about rare earth influence on other materials like silica [9], alumina [8] and Beta zeolite [10].

MCM-22 zeolite (MWW structure) is a relatively new material, synthesized by the first time in 1990 by Mobil. This material presents an original porous structure, where two independent pore systems exist, both accessible through 10-membered-ring apertures. One of the porous system has sinusoidal channels with 10-MR (4 Å × 5.0 Å). The other pore system comprises large supercages with 12-MR (7.1 Å × 18.4 Å), interconnected by 10-MR channels (4 Å × 5.5 Å). This material combines the characteristics

* Corresponding author.
E-mail address: filipa.ribeiro@ist.utl.pt (M.F. Ribeiro).

0920-5861/$ – see front matter © 2005 Elsevier B.V. All rights reserved.
doi:10.1016/j.cattod.2005.07.048

of both 10 and 12-MR zeolites. Due to this particular pore system MCM-22 has been tested for many kinds of catalytic reactions. Particularly, the potentialities of this zeolite have been tested as an additive for catalytic cracking (FCC) [11], in aromatization of *n*-butane [12], in isomerization of *m*-xylene [13] and in alkylation of benzene [14].

Beta zeolite (BEA structure) was first synthesized in 1967. It has a three-dimensional channel structure with 12-MR with elliptical openings (6.4 Å × 7.6 Å). The pore volume can be compared with that of faujasites. Because of its pore system and high acidity, it is of great potential industrial interest, especially in reactions such as catalytic cracking [15], isomerization [16,17], alkylation [18] and disproportionation [19].

The purpose of this work has been the study of the influence of rare earth elements La, Nd and Yb in the acidic properties of H-MCM-22 and H-Beta. Zeolites acidity is characterized by pyridine adsorption followed by infrared spectroscopy (FTIR) and by the model reaction of *n*-heptane cracking.

2. Experimental

MCM-22 was synthesized according to the method reported by Corma et al. [20], in a way to obtain Si/Al = 15. The as-synthesized form was calcined in air at 500 °C for 4 h. The calcined sample was ion-exchanged three times with 1 M ammonium acetate solution in order to obtain the acidic form, H-MCM-22. H-Beta zeolite was supplied by PQ Corporation with Si/Al = 12.5.

H-MCM-22 and H-Beta samples were submitted to ion exchange with rare earth nitrate solutions of La, Nd and Yb at 80 °C for 3 h in order to obtain RE/Al ratios of 0.3. After the exchange the samples were dried at 100 °C and calcined at 500 °C for 3 h under air flow of 6 L h^{-1} g^{-1} and a heating rate of 5 °C min^{-1}. These samples were named REH-MCM-22 and REH-Beta, with RE = La, Nd or Yb.

Crystallinity of all samples after the ion exchange was evaluated by X-ray powder diffraction, using a Rigaku diffractometer with Cu Kα radiation filtered by Ni. RE element contents (wt.%) were determined by ICP.

The porosity of each sample was determined by nitrogen sorption at −196 °C carried out with an automatic Micromeritics (ASAP 2010) apparatus.

The acidic properties of the samples were studied by pyridine adsorption followed by infrared spectroscopy (FTIR). The infrared spectra were recorded on a Nicolet Nexus FTIR spectrometer (60 scans, resolution 4 cm^{-1}). For IR characterization of the hydroxyl groups and of adsorbed pyridine, the zeolite samples were pressed into 12 mm diameter thin wafers (about 5 mg cm^{-2}) and evacuated at secondary vacuum (10^{-6} mbar) in situ in a IR cell at 300 °C for 8 h. After recording the initial spectrum of the sample (reference), pyridine was adsorbed at 150 °C under an equilibrium pressure of 2.7 mbar. The spectra were recorded at ambient temperature after degassing the samples for 30 min, at the required desorption temperature (150–550 °C) and using a heating rate of 5 °C min^{-1}. Band intensities were normalized by the sample weight. The background spectrum, recorded under identical operating conditions without sample, was always performed before each spectrum and automatically subtracted.

The catalytic reaction of *n*-heptane cracking was performed in a continuous flow reactor at 350 °C under a total pressure of 1 bar. Before the reaction the catalysts were pre-treated at 500 °C in situ for 10 h under nitrogen flow of 36 L h^{-1} g^{-1}. Experiments were performed for 90 min using a flow of 3 mL h^{-1} of *n*-heptane (molar ratio N_2/*n*-C_6 = 9) and WHSV = 20.5 h^{-1}. The reaction products were analyzed by an on-line gas chromatograph Hewlett-Packard 6890 series with a flame ionization detector, using a capillary column PLOT-Al_2O_3/KCl.

The coke analysis was performed by thermogravimetry using a Setaram TG-DSC92 thermobalance. Coked samples were heated under air flow with a temperature increase of 10 °C min^{-1} until 200 °C, maintaining this temperature for 1 h. Afterwards, the temperature was increased again with the same heating rate until 600 °C. The samples were cooled to room temperature and an additional heating cycle was performed under identical conditions to eliminate any fluid transport effect. The weight loss and heat profiles were obtained by subtraction of the two cycle profiles.

3. Results and discussion

3.1. Physicochemical characterization

The XRD patterns of MCM-22 were identical to those reported on literature [20]. After introduction of RE elements the XRD patterns of REH-Beta and REH-MCM-22 maintain the original crystalline structure. The unit cell formula of the samples and the microporous volumes (V_{microp}), determined by the *t*-plot method, are shown in Table 1. For all samples, the RE contents introduced are always around 10% of the predicted exchange values. For the same ion exchange conditions, NdH-MCM-22 and YbH-Beta present slightly higher contents in RE elements. H-Beta and REH-Beta show very

Table 1
Unit cell composition and microporous volumes for H-MCM-22 and H-Beta samples

Sample	Unit cell formula	V_{microp} (cm^3 g^{-1})
H-MCM-22	$H_{4.5}Al_{4.5}Si_{67.5}O_{144}$	0.164
LaH-MCM-22	$La_{0.05}H_{4.4}Al_{4.5}Si_{67.5}O_{144}$	–
NdH-MCM-22	$Nd_{0.07}H_{4.3}Al_{4.5}Si_{67.5}O_{144}$	0.134
YbH-MCM-22	$Yb_{0.04}H_{4.4}Al_{4.5}Si_{67.5}O_{144}$	0.135
H-Beta	$H_{4.7}Al_{4.7}Si_{59.3}O_{128}$	0.159
LaH-Beta	$La_{0.04}H_{4.6}Al_{4.7}Si_{59.3}O_{128}$	0.157
NdH-Beta	$Nd_{0.05}H_{4.6}Al_{4.7}Si_{59.3}O_{128}$	0.155
YbH-Beta	$Yb_{0.10}H_{4.4}Al_{4.7}Si_{59.3}O_{128}$	0.158

close values for V_{microp}, meaning that the introduction of RE elements does not affect the porosity of the samples. On the contrary, the introduction of RE elements in H-MCM-22 causes a notable decrease in V_{microp}, indicating that the presence of RE^{3+} cations causes space limitations inside H-MCM-22 porous structure.

3.2. Characterization of catalysts acidity by pyridine adsorption

Fig. 1 shows the infrared spectra of H-MCM-22 and REH-MCM-22 after pre-treatment in the range of hydroxyl stretching modes. All samples present two main bands located at 3747 and 3620 cm^{-1}. The first one corresponds to isolated silanols located on the external surfaces of the zeolite crystals [21] and the second one is attributed to bridged hydroxyl groups Si(OH)Al. At 3670 cm^{-1}, a small band can be observed that corresponds to the hydroxyl groups linked to extraframework Al species (EFAL) [22] probably generated during calcination [23]. A small increase in this band intensity is observed upon RE introduction, due to an additional calcination of these samples after ion exchange.

Fig. 2 shows the result of hydroxyl group band deconvolution for H-MCM-22, performed with "PeakFit"® software, in three components, detected by calculating the second derivative, which, according to Onida et al. [21], permit to distinguish the different locations of the acid sites in the zeolite structure. The main band around 3620 cm^{-1} is attributed to hydroxyl groups located in the supercavities, at 3605 cm^{-1} corresponds to the sinusoidal channels and at about 3577 cm^{-1} to the hexagonal prisms connecting two supercavities. The introduction of RE elements causes a decrease in the intensity of all these bands due to the substitution of H^+ by RE^{3+} cations. The band at 3620 cm^{-1} decreased about 30% for LaH-MCM-22 and NdH-MCM-22 and about 20% for YbH-MCM-22. The bands at 3605 and 3577 cm^{-1} lowered their intensity between 10 and 15% for all REH-MCM-22.

Fig. 3 shows the IR spectra of H-Beta and REH-Beta. For all samples the most intense band, located at 3745 cm^{-1}, corresponds to silanol groups. The band at 3609 cm^{-1} is attributed to the bridging hydroxyl groups. The bands at 3663 and 3781 cm^{-1} are commonly assigned to two kinds of AlOH groups in which Al atoms belong to EFAL species [24]. The introduction of RE elements causes a decrease in the 3609 cm^{-1} band due, also, to the substitution of H^+ by RE^{3+} cations.

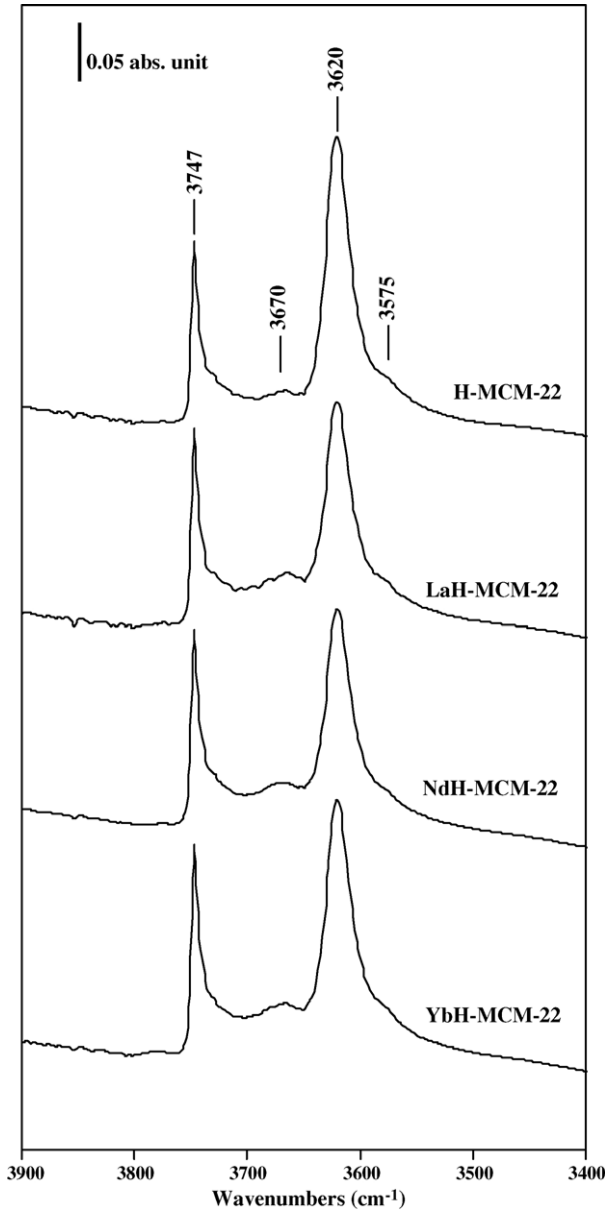

Fig. 1. Infrared spectra in the hydroxyl region of H-MCM-22 samples.

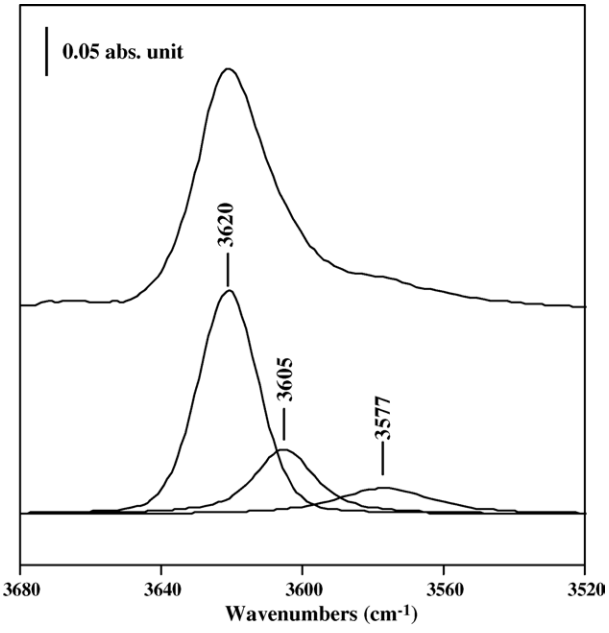

Fig. 2. Deconvolution of the hydroxyl group band for H-MCM-22.

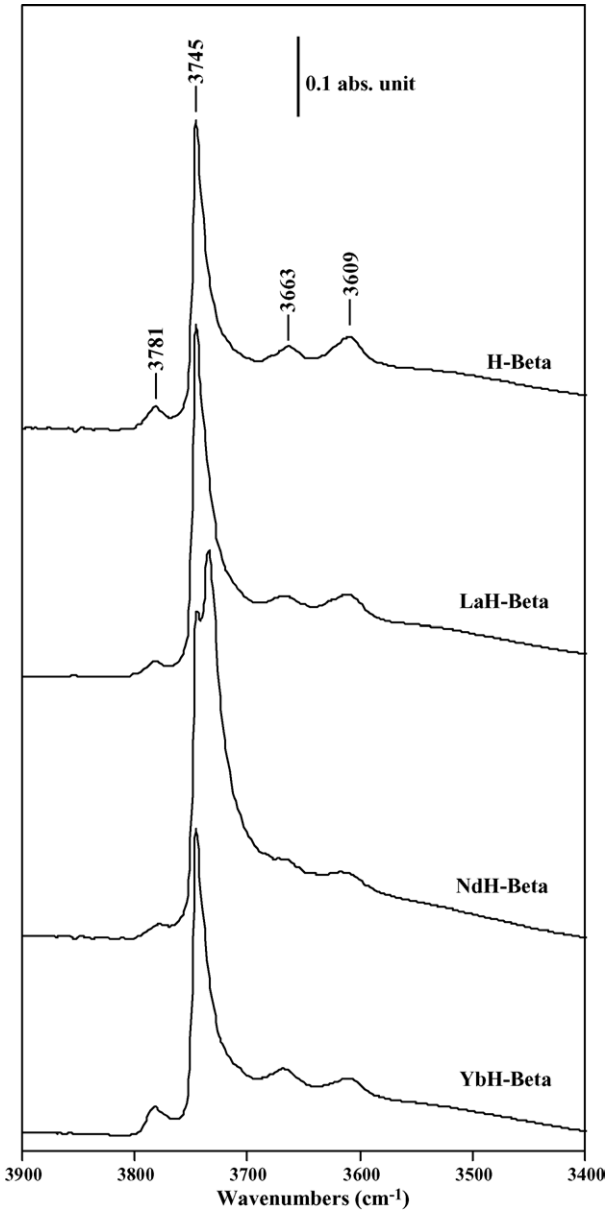

Fig. 3. Infrared spectra in the hydroxyl region of H-Beta samples.

When comparing the IR spectra for the two zeolitic structures it can be observed that the band corresponding to the bridging hydroxyl groups is always more intense in the H-MCM-22 samples, indicating a higher acid sites density.

Infrared spectra of pyridine after desorption at 150 °C in the range 1400–1700 cm^{-1} is shown in Fig. 4 for all samples. Pyridine adsorbed on H-Beta (Fig. 4A) and H-MCM-22 (Fig. 4B) results in the appearance of bands characteristic of pyridine adsorbed to Brönsted acid sites around 1544 and 1636 cm^{-1}, to Lewis acid sites at 1622 and 1455 cm^{-1} and the bands attributed to pyridine adsorbed on both Brönsted and Lewis acid sites at 1490 cm^{-1} [24,25]. In REH-MCM-22 and REH-Beta, two additional bands are also detected at 1608 and 1446 cm^{-1}. These bands have been attributed to pyridine bonded to RE^{3+} cations [26] and are related to RE–O–Al linkages originating new Lewis acid sites [9,26].

As a result of ion exchange, the RE^{3+} cations replace some of the framework protons, lowering the original acidity in both structures, which results in the observed small decrease in the intensity of the bands attributed to pyridine bonded to Brönsted acid sites. In fact, although the hydrolysis of water of solvation of RE^{3+} cations creates new Brönsted acid sites that would compensate the original acidity, the effect is not complete, as already discussed by Li et al. [27]. Nevertheless, the bands correspondent to Brönsted acid sites on H-MCM-22 samples present always higher intensity than H-Beta samples, which indicates the presence of higher Brönsted sites density.

Fig. 5 shows the infrared spectra of pyridine after desorption at 450 °C for H-MCM-22 and H-Beta, and, as an example, for YbH-MCM-22 and YbH-Beta. All samples are able to retain pyridine bonded to Lewis acid sites after desorption at 450 °C. Additional bands corresponding to new Lewis sites are also visible, which reveals the presence of strong acid sites. The bands characteristics of Brönsted acid sites are visible after pyridine desorption at 450 °C for H-MCM-22 and H-Beta. The introduction of RE elements on H-MCM-22 has no effect on the strength of Brönsted acid sites because the corresponding bands remain visible after pyridine desorption at 450 °C. For REH-Beta, the bands attributed to Brönsted sites are no longer detected, as shown for YbH-Beta.

3.3. *n*-Heptane cracking

The effect of RE introduction on acidity was evaluated by the model reaction of *n*-heptane cracking. Table 2 resumes the main parameters related to this reaction for all samples after 5 and 90 min time on stream.

For all samples, the main reaction products are hydrocarbons (olefins and paraffins) with three and four carbon atoms ($C_3 + C_4$). Some isomerization and aromatization products are also detected, with percentages around 10 and 5%, respectively, for H-Beta and 5 and 2% for H-MCM-22 samples. Light products with one and two carbon atoms (C_1 and C_2) are detected with values below 0.2% for Beta zeolite samples and around 1–2% for H-MCM-22 samples.

Fig. 6 show the evolution of catalytic activity with time on stream for both zeolites. The initial activities (at $t = 5$ min) for H-Beta and H-MCM-22 are very close. After RE introduction, the activity decreases for all REH-Beta and REH-MCM-22, being this effect more pronounced for both Nd samples. The catalysts deactivation is higher for H-Beta and REH-Beta, as can be observed from ΔConv. values in Table 2.

The ratio olefins/paraffins (O/P), quantified for products with four carbon atoms (C_4), measures the hydrogen transfer ability of the zeolite catalysts. As the hydrogen transfer reaction follows a bimolecular mechanism it is favored by a

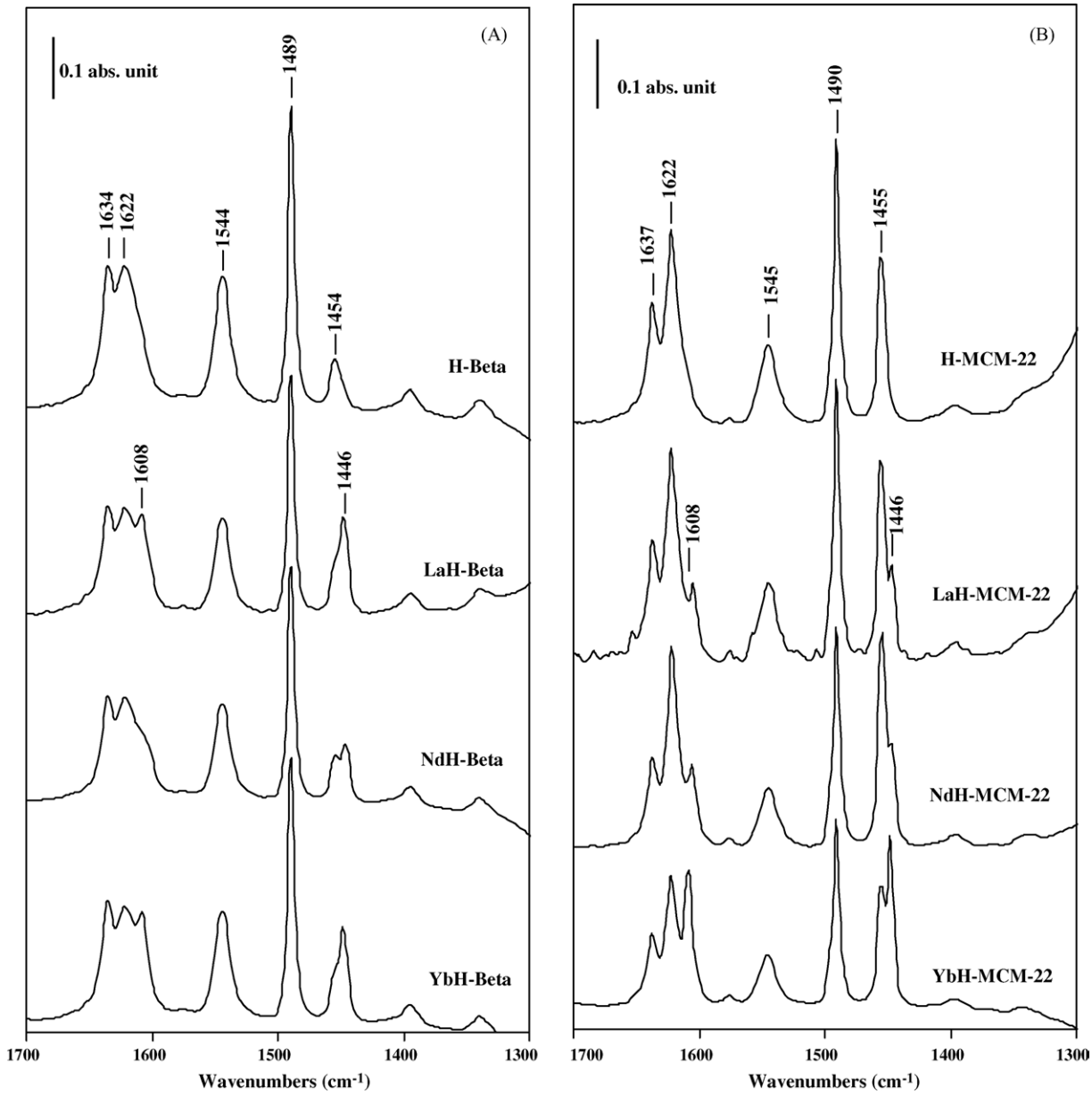

Fig. 4. Infrared spectra of pyridine after desorption at 150 °C for (A) H-MCM-22 and (B) H-Beta samples.

high density of Brönsted acid sites [28]. The lower value of the ratio O/P observed in H-MCM-22 indicates a higher consumption of olefins, what means that this sample has a higher acid site density than H-Beta.

The introduction of RE elements on H-Beta zeolite decreases the O/P ratio in this zeolite, due to olefins conversion into aromatic compounds, which justifies the higher percentage in aromatics verified in REH-Beta and also a more pronounced deactivation observed in these catalysts. This result was already observed for Y zeolite by Scherzer [1] and Pine et al. [5] that attributed the increase in hydrogen transfer to the presence of rare earth ions. In fact, the presence RE cations origins new Lewis acid sites, as already discussed in the IR results and, although the importance of Lewis acid sites in cracking reactions is not clear, some authors believe that Lewis sites can play an active role in these reactions [29]. Other authors postulate a synergistic effect between Brönsted and Lewis acid sites, claiming that the role of Lewis sites is to increase the acid strength of the OH groups, through a raise in the ionic field located in RE cations vicinity [30,31].

REH-MCM-22 samples show a different behavior, being the O/P ratio slightly higher than on H-MCM-22, probably because of the most difficult access to the places with higher acid sites density (supercavities) due to the presence of the bulky RE cations in the access channels that are responsible for geometric constraints.

The branched to linear products ratio (B/L), also calculated for C_4 products, is related not only with catalyst acidity [32] but also with the available space inside the

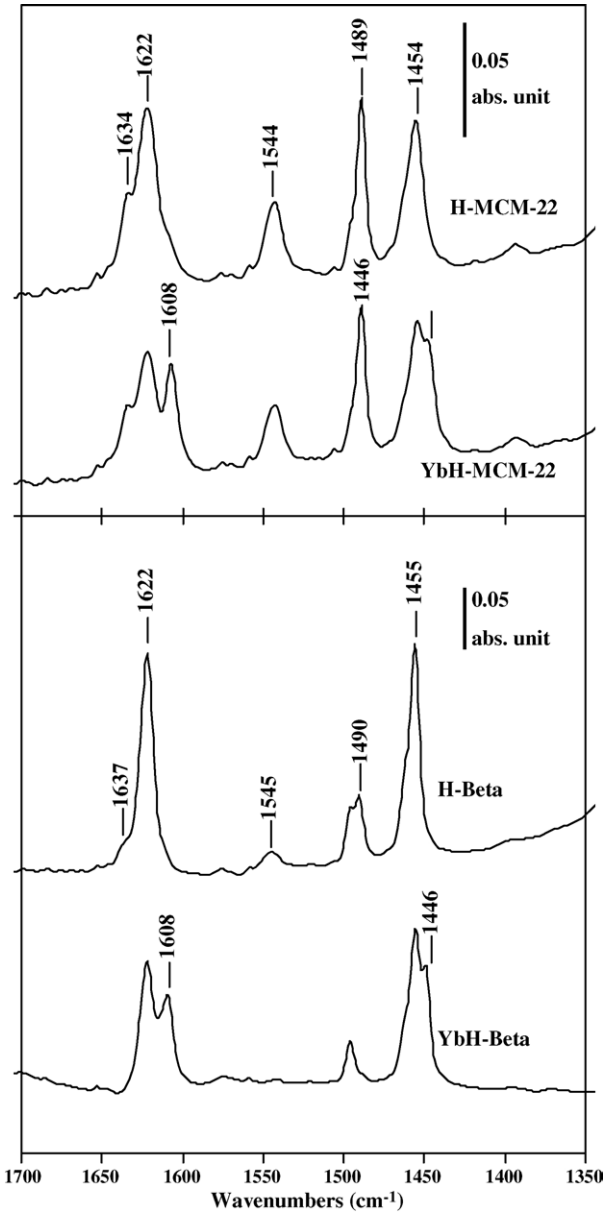

Fig. 5. Infrared spectra of pyridine after desorption at 450 °C.

catalyst porous structure. The introduction of RE elements in H-MCM-22 leads to a decrease in B/L ratio because the rare earth cations have a shape selectivity effect on MCM-22, as shown by the decrease in the microporous volume (Table 1) that privileges the formation of linear products. This shape selectivity effect does not seem to be present on REH-Beta samples, even on the catalysts containing the cation with higher ionic radius, La, due to the larger dimensions of H-Beta porous structure.

The ratio between light products ($C_1 + C_2$) and isobutane, ($C_1 + C_2$)/*i*-C_4, is considered a good indicator of the ratio between protolytic to β-scission mechanism [33]. This ratio shows very low values for H-Beta and REH-Beta (see Table 2), meaning that cracking reactions occur mainly according to β-scission mechanism. For H-MCM-22 and

Table 2
Catalytic behavior of H-MCM-22 and H-Beta samples in *n*-heptane cracking after 5 and 90 min time on stream

Catalyst	Conv. (%)	O/P (C_4)[a]	B/L (C_4)[b]	($C_1 + C_2$)/ *i*-C_4	ΔConv.[c]	Coke (wt.%)
H-MCM-22	27	0.18	3.6	0.15	13	
	(14)	(0.40)	(1.9)	(0.56)		5.0
LaH-MCM-22	25	0.28	2.8	0.28	10	
	(15)	(0.36)	(2.1)	(0.41)		4.8
NdH-MCM-22	19	0.23	3.2	0.22	9	
	(10)	(0.46)	(1.9)	(0.60)		4.2
YbH-MCM-22	24	0.25	3.2	0.18	8	
	(16)	(0.39)	(2.0)	(0.38)		4.5
H-Beta	29	0.37	3.9	0.05	19	
	(10)	(0.45)	(3.6)	(0.16)		4.8
LaH-Beta	24	0.17	4.1	0.05	17	
	(7)	(0.42)	(3.9)	(0.13)		6.2
NdH-Beta	18	0.17	4.0	0.06	12	
	(6)	(0.38)	(3.9)	(0.16)		5.6
YbH-Beta	25	0.16	4.4	0.03	15	
	(10)	(0.37)	(4.3)	(0.07)		6.8

[a] Olefins to paraffin ratio calculated for compounds with four carbon atoms.
[b] Branched to linear ratio calculated for compounds with four carbon atoms.
[c] Variation in the conversion calculated by the difference between the values at 5 and 90 min time on stream.

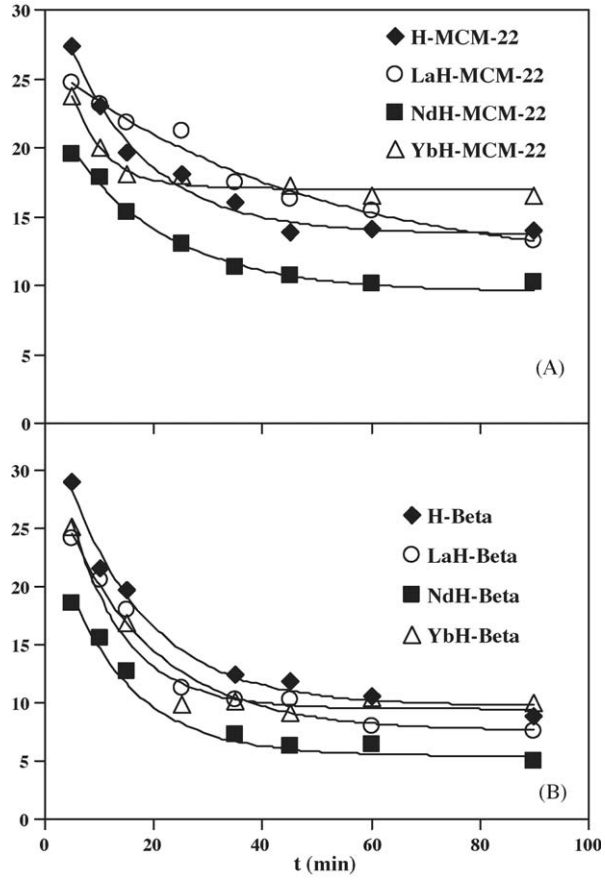

Fig. 6. Catalytic conversion for *n*-heptane cracking at 350 °C for (A) H-MCM-22 and (B) H-Beta samples.

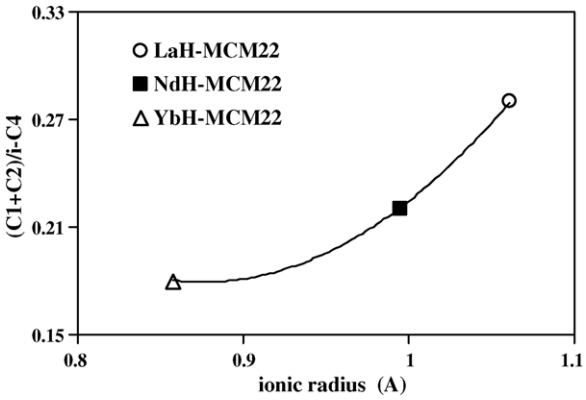

Fig. 7. Evolution of the ratio between light products and isobutane with the ionic radius of rare earth elements for REH-MCM-22 samples.

REH-MCM-22, the ratio $(C_1 + C_2)/i\text{-}C_4$ presents higher values which means that the protolytic cracking mechanism has a higher contribution. These results can be explained attending that the bi-molecular β-scission mechanism evolves bulky transition states, when compared to the mono-molecular protolytic mechanism, being fundamental the pore diameter and the porous structure of the catalyst [33,34]. Attending to the space limitations imposed by the presence of RE^{3+} cations, as showed by the decrease in V_{microp}, REH-MCM-22 samples show a raise in light products, characteristic of protolytic cracking. Fig. 7 shows an increases of light products with the ionic radius of the RE element introduced, La > Nd > Yb. Additionally, it is known that protolytic cracking occurs exclusively over strong Brönsted acid sites [35] because the energy of the activation step is higher than that of bimolecular cracking [36] which is in accordance to the presence of stronger Brönsted acid sites detected by pyridine adsorption on REH-MCM-22 when compared to REH-Beta.

3.4. Coke deposition

During *n*-heptane cracking reaction coke deposition takes place. The coke contents on used catalysts were analyzed by TG and are reported on Table 2. It is noteworthy that coke contents present comparable values for all samples, although the contents for H-Beta samples are slightly higher. The DSC profiles obtained burning the coke deposited on the used samples reveals some differences. Fig. 8 shows the heat flow profiles for H-Beta and H-MCM-22. There are three distinct zones on H-MCM-22 heat profile, the first at 250 °C, the second around 350 °C and the third at 500 °C. These different zones in the DSC profiles are certainly due the different composition of coke, which depends very much on its location [37]. The particular structure of MCM-22 zeolite favors the deposition of different types of coke. According to Meloni et al. [34] the protonic sites of the supercages are rapidly deactivated owing to a fast formation and retention of coke molecules in these trap cages. On the contrary, deactivation of the protonic sites of the sinusoidal channels

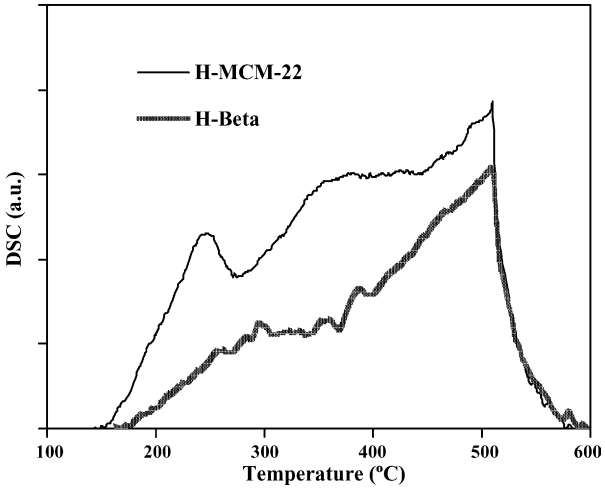

Fig. 8. Heat flow profiles obtained during coke burning for H-MCM-22 and H-Beta.

is very slow. Consequently, coke deposited on the supercages is constituted of highly dehydrogenated polyaromatic molecules. In the sinusoidal channels only naphthalene molecules are retained, due to trapping in the small cages along the channels. The presence of this type of coke, less dehydrogenated and more reactive is responsible for the appearance of low temperature bands in the DSC profiles for H-MCM-22. H-Beta heat profile shows a small band around 300 °C and an intense signal at 500 °C, which corresponds to highly dehydrogenated polyaromatic molecules, which is in agreement with the higher deactivation observed for this catalyst.

The influence of RE introduction on DSC profiles for H-MCM-22 samples is showed in Fig. 9. The most relevant observation in the heat profiles for REH-MCM-22 is the disappearance of the low temperature band, which corresponds to the most reactive coke, meaning that the introduction of the RE^{3+} cations partially blocks the

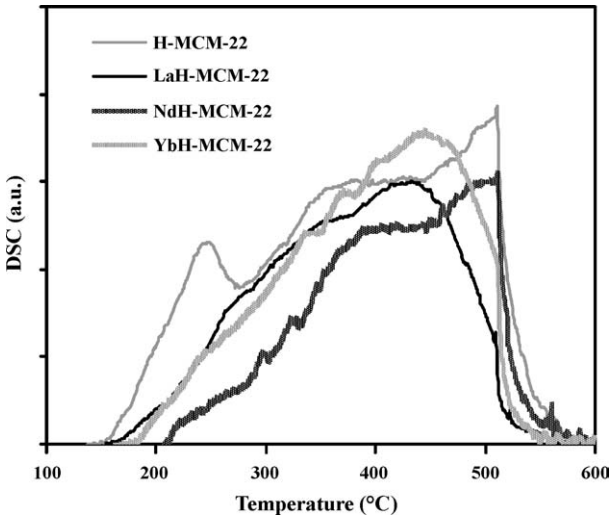

Fig. 9. Heat flow profiles of coke burning for H-MCM-22 and REH-MCM-22.

sinusoidal channels and the coke deposits are mainly located in the supercages. The heat profiles for REH-Beta show the same zones as for H-Beta, meaning that the localization of coke deposits remains unchanged after RE^{3+} introduction.

4. Conclusions

The purpose of this work was to study the influence of rare earth elements La, Nd and Yb on the acidity properties of two zeolites with distinct structures, H-MCM-22 and H-Beta.

The spectra of pyridine adsorption followed by FTIR show the presence of new Lewis acid sites in both structures, attributed to pyridine bonded to RE^{3+} cations.

The results obtained with *n*-heptane cracking reaction show that the introduction of RE elements has a distinct effect in the two zeolites that is directly related with the acidity and the porous structure of both zeolites. In H-Beta zeolite, the RE introduction enhances the catalyst acidity leading to an increase of branched products. Moreover, the occurrence of hydrogen transfer reaction leads to a higher deactivation of these catalysts, by coke formation.

The introduction of RE elements in H-MCM-22 has a small influence on catalysts acidity. The main effect was observed on shape selectivity that becomes more pronounced with the ionic radius of the RE introduced. In this zeolite, where the pores and cavity openings have small dimensions, the protolytic cracking acquires a more relevant importance, when compared with H-Beta and REH-Beta samples.

The DSC curves, corresponding to coke burning, show different energy profiles on the two materials, which are related to its porous structure, with more reactive coke for H-MCM-22. The RE introduction causes modifications on the heat flow profiles of REH-MCM-22 due to geometrical limitations imposed by the presence of RE^{3+} cations that confine the coke deposits mainly to the supercages.

References

[1] J. Scherzer, R.E. Ritter, Ind. Eng. Chem. Res. Dev. 17 (1978) 219.
[2] F. Lemos, J.M. Lopes, F. Ramôa-Ribeiro, E. Derouane, Appl. Catal. 49 (1989) 175.
[3] G. de la Puente, U. Sedran, Appl. Catal. A: Gen. 144 (1996) 147.
[4] F.N. Guerzoni, J. Abbot, Appl. Catal. A: Gen. 127 (1995) 41.
[5] L.A. Pine, P.J. Maher, W.A. Wachter, J. Catal. 85 (1984) 466.
[6] G. de la Puente, E.F. Souza-Aguiar, F.M.Z. Zotin, V.L.D. Camorin, U. Sedran, Appl. Catal. A: Gen. 197 (2000) 41.
[7] T. Baba, R. Koide, Y. Ono, J. Chem. Soc., Chem. Commun. 10 (1991) 691.
[8] T. Yamamaoto, T. Tanaka, T. Matsuyama, T. Funabiki, S. Yoshida, J. Phys. Chem. B 105 (2001) 1908.
[9] G.A.H. Mekhemer, Phys. Chem. Chem. Phys. 4 (2002) 5400.
[10] C. Jia, P. Massiani, P. Beaunier, D. Barthomeuf, Appl. Catal. A: Gen. 106 (1993) L185.
[11] A. Corma, J. Martinez-Triguero, J. Catal. 165 (1997) 102.
[12] N. Kumar, R. Byggnigsbacka, M. Korpi, L.-E. Linfors, T. Salmi, Appl. Catal. A: Gen. 227 (2002) 97.
[13] R. Ravishankar, D. Bhattachrya, N.E. Jacob, S. Sivasanker, Micropor. Mater. 4 (1995) 83.
[14] A. Corma, V. Martinez, E. Schnoevelt, J. Catal. 192 (2000) 163.
[15] A. Corma, V. Fornés, J.B. Monton, A.V. Orchilés, J. Catal. 107 (1987) 288.
[16] T. Yashima, Z.B. Wang, A. Kamo, T. Yoneda, T. Komatsu, Catal. Today 29 (1996) 279.
[17] J.-K. Lee, H.-K. Rhee, Catal. Today 38 (1997) 141.
[18] M. Hon, S.X. Lin, E. Roduner, Appl. Catal. A: Gen. 243 (2003) 175.
[19] A.B. Halgeri, J. Das, Appl. Catal. A: Gen. 181 (1999) 347.
[20] A. Corma, C. Corell, V. Fornés, W. Kolodzieski, J. Péres-Pariente, Zeolites 15 (1995) 2.
[21] B. Onida, F. Geobaldo, F. Testa, F. Crea, E. Garrone, Micropor. Mesopor. Mater. 30 (1999) 119.
[22] K. Okumura, M. Hashimoto, T. Mimura, M. Niwa, J. Catal. 206 (2002) 23.
[23] E. Bourgeat-Lami, P. Massiani, F. Di Renzo, P. Espiau, F. Fajula, Appl. Catal. 72 (1991) 139.
[24] J.P. Marques, I. Gener, P. Ayrault, J.C. Bordado, J.M. Lopes, F. Râmoa Ribeiro, M. Guisnet, Micropor. Mesopor. Mater. 60 (2003) 251.
[25] M. Guisnet, P. Ayrault, C. Coutanceau, M.F. Alvarez, J. Chem. Soc. Faraday Trans. 93 (1997) 1661.
[26] S.É. Spiridonov, K.S.U. Nasukhanov, O.V. Kryukov, E.B. Podyacheva, Kinet. Catal. 33 (1992) 317.
[27] D. Li, F. Li, J. Ren, Y. Sun, Appl. Catal. A: Gen. 241 (2003) 15.
[28] M.I. Poutsma, in: J.A. Rabo (Ed.), Zeolite Chemistry and Catalysis, ACS Monograph 171, American Chemical Society, Washington, DC, 1976, p. 680.
[29] J.W. Ward, J. Catal. 10 (1968) 34.
[30] J.H. Lunsford, J. Phys. Chem. 72 (1968) 4163.
[31] P.D. Hopkins, J. Catal. 12 (1968) 325.
[32] A. Corma, A.V. Orchillés, J. Catal. 115 (1989) 551.
[33] A. Corma, A.V. Orchillés, Micropor. Mesopor. Mater. 35 (2000) 21.
[34] D. Meloni, D. Martin, M. Guisnet, Appl. Catal. A: Gen. 215 (2001) 67.
[35] A. Brait, K. Seshan, H. Weinstbl, A. Ecker, J.A. Lercher, Appl. Catal. A: Gen. 169 (1998) 315.
[36] G. de la Puente, U.A. Sedran, J. Catal. 179 (1998) 36.
[37] M. Guisnet, P. Magnoux, Appl. Catal. 54 (1989) 1.